NASA TECHNICAL MEMORANDUM

NASA TM X-2112

NASA TM X-2112

PERFORMANCE OF CONVERGENT AND PLUG NOZZLES AT MACH NUMBERS FROM 0 TO 1.97

by Douglas E. Harrington

Lewis Research Center

Cleveland, Ohio 44135

NATIONAL AERONAUTICS AND SPACE ADMINISTRATION • WASHINGTON, D. C. • OCTOBER 1970

1. Report No. NASA TM X-2112	2. Government Accession No.	3. Recipient's Catalog No.
4. Title and Subtitle PERFORMANCE OF CONVERGENT AND PLUG NOZZLES AT MACH NUMBERS FROM 0 TO 1.97		5. Report Date October 1970 6. Performing Organization Code
7. Author(s) Douglas E. Harrington		8. Performing Organization Report No. E-5588
9. Performing Organization Name and Address Lewis Research Center National Aeronautics and Space Administration Cleveland, Ohio 44135		10. Work Unit No. 720-03 11. Contract or Grant No. 13. Type of Report and Period Covered Technical Memorandum
12. Sponsoring Agency Name and Address National Aeronautics and Space Administration Washington, D. C. 20546		14. Sponsoring Agency Code

15. Supplementary Notes

16. Abstract

A parametric variation of projected boattail area and plug area was conducted to determine the effect on performance characteristics. A convergent nozzle with a circular arc boattail and a jet to nacelle area ratio of 0.25 had an efficiency of 98.2 percent at a subsonic cruise Mach number of 0.90 and a nozzle pressure ratio of 2.8. At the same conditions a plug nozzle with a circular arc boattail and a small plug had an efficiency of 97.3 percent, while a large-plug nozzle without a boattail was 93.9 percent efficient.

17. Key Words (Suggested by Author(s))	18. Distribution Statement
Exhaust nozzle systems Convergent nozzles Plug nozzles Boattail	Unclassified - unlimited

19. Security Classif. (of this report)	20. Security Classif. (of this page)	21. No. of Pages	22. Price*
Unclassified	Unclassified	36	$3.00

*For sale by the Clearinghouse for Federal Scientific and Technical Information Springfield, Virginia 22151

PERFORMANCE OF CONVERGENT AND PLUG NOZZLES AT MACH NUMBERS FROM 0 TO 1.97

by Douglas E. Harrington

Lewis Research Center

SUMMARY

A parametric variation of projected boattail area and plug area was conducted to determine the effect on performance characteristics. Three basic nozzles were tested: a convergent nozzle with a circular arc boattail, a conical plug nozzle with a large plug and no boattail, and a conical plug nozzle with a small plug and a circular arc boattail. The small-plug nozzle was designed such that the projected boattail and plug areas were equal. Each of these nozzles had a throat area that was 25 percent of the nacelle area. Two additional convergent nozzles were tested to evaluate effects of throat area variations. Testing was conducted over a range of Mach numbers from 0 to 1.97.

At a subsonic cruise Mach number of 0.90 and a nozzle pressure ratio of 2.8, the convergent nozzle with a jet to nacelle area ratio of 0.25 provided better efficiency than either of the two conical plug nozzles. For example, the convergent nozzle had an efficiency of 98.2 percent compared with 97.3 percent for the small-plug nozzle and 93.9 percent for the large-plug nozzle. The high performance of the convergent nozzle was a result of the low boattail pressure drag. At subsonic speeds the recompression at the trailing edge of the long circular arc boattail resulted in essentially zero boattail drag up to Mach 0.95. The plug force of the small-plug nozzle was generally near zero at subsonic speeds but the boattail had a small drag which resulted in slightly lower performance when compared with the convergent nozzle. The low performance of the large-plug nozzle can be directly attributed to the large drag on the plug surface.

At a supersonic dash Mach number of 1.97 and a nozzle pressure ratio of 10.7 the convergent nozzle with a jet-area-to-nacelle-area ratio of 0.35 provided a peak efficiency of 90.5 percent. At this flight condition the boattail drag accounted for a 2 percent loss in nozzle efficiency.

INTRODUCTION

Exhaust nozzles for multimission fighter aircraft are designed primarily for high subsonic cruise efficiency but also must have good efficiency for supersonic dash. At subsonic cruise, the nozzle throat area may be only 25 percent of the maximum nacelle area. The problem then arises as to what should be done with the remaining 75 percent of the nacelle area which projects rearward in the drag direction. This is particularly critical at subsonic cruise since the engine is at a lower power setting and the net thrust is low. Nacelle drag can therefore be a large percentage of the net thrust if not treated properly. Two extreme cases can be considered. In the first case a convergent nozzle can be used so that the remaining 75 percent of the nacelle area is a large boattail. Considerable attention must then be given to the design of the boattail in order to keep the afterbody drag to a minimum. The other case would be to use a large-plug nozzle with a cylindrical nacelle. Thus, the remaining 75 percent of the nacelle area would be plug area.

This report presents the results of a brief experimental investigation of a parametric variation between projected boattail area and plug area. Testing was conducted in the Lewis 8- by 6-Foot Supersonic Wind Tunnel over a range of Mach numbers from 0 to 1.98. Three basic nozzle configurations were tested: a convergent nozzle with a circular arc boattail, a conical plug nozzle with a large plug and no boattail, and a conical plug nozzle with a small plug and a circular arc boattail. The small-plug nozzle was designed such that the projected boattail and plug areas were equal. Each of these nozzles had a throat area that was 25 percent of the nacelle area. Two additional convergent nozzles were tested to evaluate effects of throat area variations.

APPARATUS AND PROCEDURE

Installation

The isolated nacelle was strut mounted in the test section of the Lewis 8- by 6-Foot Supersonic Wind Tunnel as shown in figure 1. The geometry of the model and its thrust-measuring system are shown in figure 2. The main part of the model was a strut-supported cylinder with a closed nose. The model external shell was grounded and was supported from the tunnel ceiling by a hollow, vertical strut. The floating portion of the model was attached to the air bottle, which was cantilevered by flow tubes from supply manifolds located outside the test section. Front and rear bearings supported the air bottle. Thus, the axial force acting on the floating part of the model, including both the adapter and nozzle sections, was transmitted to the load cell located in the nose of the

model shell. Although the friction drag on the floating portion of the model, designated as the adapter, was measured by the load cell, the data were adjusted so that it was not included in the nozzle efficiency parameter. This friction drag on the adapter was estimated by using the semiempirical, flat plate, local skin-friction coefficient (given in fig. 6 of ref. 1) as a function of free-stream Mach number and Reynolds number. The coefficient accounts for variations in boundary-layer thickness and flow profile with Reynolds number. Previous measurements of the boundary-layer characteristics at the aft end of this jet-exit model (ref. 2) indicated that the profile and the thickness were essentially the same as that computed for a flat plate of equal length. The average ratio of boundary-layer momentum thickness to model diameter was computed to be approximately 0.02. The strut wake appeared to affect only a localized region near the top of the model and resulted in a lower local free-stream velocity than measured on the side and bottom of the model. Therefore, the results of reference 1 were used without correction for three-dimensional flow effects or strut interference effects. The calculated friction drag of the adapter section was added to the load-cell reading to obtain the thrust-minus-drag of the nozzle section.

A static calibration of the thrust-measuring system was obtained by applying a known force to the nozzle and measuring the output of the load cell. To minimize changes in the calibration due to variations in temperature (e.g., aerodynamic heating due to external flow), the load cell was surrounded by a water-cooled jacket and was maintained at a constant temperature.

Primary air was provided by means of airflow supply lines which entered the model through the support strut. Uniform flow was maintained by using two choke plates and an airflow straightener upstream of station 7. Primary weight flow was determined from a standard ASME flowmetering orifice located in the main air supply line. The ambient pressure was a constant for a given free-stream Mach number; thus, a variation in nozzle pressure ratio was obtained by varying the nozzle inlet pressure P_7.

Nozzle Geometry

The various nozzles tested are shown in figure 3, and the dimension and geometric variables are given in detail in figure 4. Three basic nozzle configurations were tested. The first configuration was a convergent nozzle with a large circular arc boattail and is shown in figure 4(a). This nozzle had a throat-area-to-nacelle-area ratio A_8/A_m of 0.25. The remaining projected nacelle area was devoted to the boattail and small annular base area. The boattail radius of curvature was 7.5 model diameters and the boattail trailing-edge angle was 14.5°. The second configuration was a large-plug nozzle with a cylindrical nacelle (i.e., no boattail) and is shown in figure 4(b). As with the

previous convergent nozzle, this nozzle had a throat-to-nacelle area ratio of 0.25. The remaining projected nacelle area was devoted to the plug and small annular base area of the cylindrical nacelle. The plug was conical, with a 10° half angle, and was supported by three struts equally spaced circumferentially. The throat of this plug nozzle was located on the shoulder of the plug and was normal to the plug axis. The third nozzle, shown in figure 4(c), had a small plug and was a compromise between the first two nozzles. The throat-area-to-nacelle-area ratio was again 0.25. The remaining projected nacelle area was divided equally between the nacelle boattail (including the small annular base area) and the plug surface downstream of the throat. The boattail radius of curvature was 8.5 model diameters and the trailing-edge angle was 9°. The plug was conical, with a 10° half angle, and was supported by three struts equally spaced circumferentially. The throat of this plug was also normal to the plug axis. Two additional convergent nozzles were tested to simulate throat area variations and are shown in figure 4(d). One configuration had a throat-area-to-nacelle-area ratio of 0.35, a boattail radius of curvature of 7.5 model diameters, and a boattail trailing-edge angle of 13.3°. A throat-area-to-nacelle-area ratio of 0.50 may have been more realistic for an afterburning turbofan engine at high power settings, but due to model flow limitations this size throat was unattainable. The other configuration had a throat-area-to-nacelle-area ratio of 0.10, a boattail radius of curvature of 7.5 model diameters, and a boattail trailing-edge angle of 17.3°. A summary of nozzle variables is given in table I.

Instrumentation

Nozzle static-pressure instrumentation for all configurations is presented in figure 5. The boattails of the convergent nozzles were instrumented with three rows of 10 static-pressure orifices each (fig. 5(a)). These rows were located at 0°, 90°, and 180° circumferentially (looking upstream). The pressure drag of these boattails was determined by assigning an area to each orifice and then performing a pressure-area integration over the entire boattail surface. The boattail of the small plug (fig. 5(b)) was instrumented in the same manner and the drag determined as before. Plug pressure instrumentation included three rows of 11 static-pressure orifices each (figs. 5(b) and (c)). These rows were located at 0°, 90°, and 180° circumferentially (looking upstream). The orifices in each row were located at the centroids of equal projected areas. The plug force was then determined by pressure-area integration. Orifice 1 was not included in the plug force calculation but was used to determine the throat pressure. The annular bases of the various nozzles were instrumented with three static-pressure orifices. These were located at 5°, 95°, and 185° circumferentially. Base pressure was assumed to be the average of these pressures. No attempt was made to determine the force due

to friction on either the boattails or plugs.

Details of pressure instrumentation at station 7 are shown in figure 6. Pressures in the primary airflow assage were measured by two static-pressure orifices and a total-pressure rake containing 11 probes. Primary nozzle total pressure was obtained from an integrated average of these pressures. The accompanying table lists pressure orifice spacing as distance y from the inner surface of the passage.

Procedure for Calculating Nozzle Efficiency for the Convergent Nozzle, $A_8/A_m = 0.10$

Figure 7 presents a comparison of measured and theoretical internal performance of the two larger convergent nozzles. The measured values of internal performance were obtained for these nozzles with $A_8/A_m = 0.25$ and 0.35 by adding the boattail and base pressure drag to the thrust-minus-drag measured by the load cell. The measured internal performance was slightly higher than ideal but generally within a percent of the theoretical value. Due to the small throat of the convergent nozzle with $A_8/A_m = 0.10$, the primary weight flow and load-cell forces were quite low and thus the accuracy of the various measurement systems was questionable for this configuration. As a consequence, it was decided that rather than using the load-cell forces to determine nozzle efficiency for this configuration, the efficiency would be calculated by using the ideal internal performance of a convergent nozzle and the measured external pressure drag forces. No allowance was made for external skin-friction drag in these calculations.

Wind Tunnel Interference Effects

Pressure disturbances resulting from tunnel blockage effects and support interference effects can greatly influence the measured performance of an exhaust nozzle system. This is particularly true of the nozzles tested in the present study because of the large projected areas exposed to the external stream. Reference 3 indicates that the region of largest pressure disturbances occurs from Mach 1.1 to Mach 1.47 for this particular jet-exit model. Hence, no data are presented in this Mach number range except at $M_0 = 1.47$ for the convergent nozzles with $A_8/A_m = 0.25$ and 0.35. It was felt that the boattail drag of these configurations was low enough so that any pressure disturbances caused by blockage or support interference would only have a small effect on overall performance.

RESULTS AND DISCUSSION

In order to facilitate a comparison of the various nozzles tested, a nozzle pressure ratio schedule was assumed for a typical turbofan engine designed for multimission fighter aircraft. This schedule is presented in figure 8. The subsonic cruise point was chosen to be Mach 0.90 and a pressure ratio of 2.8.

Nozzle performance characteristics are compared for this assumed nozzle pressure ratio schedule in figures 9 to 12. The effect of variations in nozzle pressure ratio on performance is presented next in figures 13 to 16. Figures 17 and 18 include plug and boattail pressure distributions at a number of selected Mach numbers and pressure ratios.

Nozzle Performance Characteristics Over the Assumed Trajectory

A comparison of performance characteristics of the plug nozzles and a convergent nozzle is presented in figure 9 using the assumed turbofan pressure ratio schedule. These nozzles had a throat-area-to-nacelle-area ratio A_8/A_m of 0.25.

At a subsonic cruise Mach number of 0.90 and a nozzle pressure ratio of 2.8, the convergent nozzle with $A_8/A_m = 0.25$ provided better efficiency than either of the other two plug nozzles tested (fig. 9(a)). This nozzle had an efficiency of 98.2 percent, while the small plug had an efficiency of 97.3 percent and the large plug had the lowest efficiency, 93.9 percent.

The high performance of the convergent nozzle was a result of the very low boattail pressure drag (fig. 9(b)). At subsonic speeds the recompression at the trailing edge of the long circular arc boattail was enough to result in essentially zero boattail drag up to Mach 0.96. The plug force of the small-plug nozzle was generally near zero at subsonic speeds but the boattail had a small drag, providing slightly lower overall performance. As mentioned previously, this nozzle had an axially directed throat. It can be seen in figure 9(b) that the drag on the boattail of the small-plug nozzle was higher at subsonic speeds than the drag of the boattail for the convergent nozzle even though its projected area was less. This increased drag for the short boattail resulted from the loss of the recompression at the trailing edge of the longer boattail. The low performance of the large-plug nozzle can be directly attributed to the large drag on the plug surface at all Mach numbers tested. This nozzle also had an axially directed throat.

Figure 10 presents the effect of throat area variation on performance characteristics of the convergent nozzles using the assumed turbofan pressure ratio schedule. For the reason mentioned previously the nozzle efficiencies of the convergent nozzle with $A_8/A_m = 0.10$ were calculated by subtracting the boattail and base pressure drag from

the ideal internal thrust of a convergent nozzle. No allowance was made for boattail skin friction drag in this calculation.

At subsonic speeds the boattail drag for these configurations is essentially zero. Hence, the nozzle efficiency remains high since a convergent nozzle is very efficient at the low values of nozzle pressure ratio assumed for the trajectory. At supersonic speeds the overall nozzle efficiency again was sensitive to the boattail drag. The convergent nozzle with $A_8/A_m = 0.35$ had an efficiency of 90.5 percent at Mach 1.97 since its boattail drag only accounted for a 2 percent loss in overall efficiency. The ideal internal performance of a convergent nozzle at this flight condition would provide a nozzle efficiency of about 92.4 percent, as shown in figure 10(a). (As mentioned previously a more realistic throat-area-to-nacelle-area ratio would be 0.50 for an afterburning turbofan engine at supersonic speeds. It would appear that a configuration like that would attain a nozzle efficiency close to 92 percent at Mach 1.97 since boattail drag would be negligible compared to the ideal thrust.)

Figure 11 presents a comparison of efficiencies between the plug nozzles of the present study and several similar plug nozzles. These comparisons were made using the assumed turbofan pressure ratio schedule. In addition, all these nozzles were tested with primary air only and either a retracted external shroud or no external shroud at all. The key to figure 11 lists some of the more important parameters for these nozzles. The small-plug nozzle consistently had comparable or higher efficiencies than did any of the other plug nozzles used in this comparison. This resulted because the low-angle circular arc boattail kept the boattail drag to a minimum and placed the plug in a favorable flow recompression region. The plug nozzle tested in reference 4 was very similar to the small-plug nozzle in the present study, as can be seen from the key. The major differences were that the plug nozzle in reference 4 had an internal lip angle of 6°, a 1° tapered nacelle, and a 4.5° conical boattail. Nozzle efficiencies for both nozzles were comparable at all subsonic Mach numbers, except at takeoff where the small-plug nozzle was 2 percent higher. The plug nozzle reported in reference 5 also had efficiencies that were comparable to those of the small-plug nozzle at all subsonic Mach numbers. This nozzle (ref. 5) had a much larger plug than did the small-plug nozzle. However, it did have an internal expansion ratio A_9/A_8 of 1.12 which forced the primary flow down the plug surface. This reduced the overexpansion region on the plug surface just downstream of the throat which was evident on the large plug of the current test. The boattail on the small plug helped prevent this initial overexpansion on the plug surface. Thus the internal expansion compensated for the smooth boattail, and efficiency was maintained at a relatively high level.

The large-plug nozzle had efficiencies that were comparable to the plug nozzle reported in reference 6, except at subsonic cruise where the large-plug nozzle efficiency was several percent higher. Both had lower efficiencies than the previously discussed

nozzles. The large-plug nozzle and the nozzle in reference 6 are quite similar in that they both have large plugs and no internal expansion. However, the nozzle in reference 5 has an 8° internal lip angle, while the large-plug nozzle has an axial throat. Any advantage of the inclined throat, however, was apparently cancelled by the drag on the base and boattail inherent in the design of the inclined throat nozzle.

Figure 12 presents a comparison of boattail pressure drag coefficients for the boattailed nozzles using the assumed turbofan pressure ratio schedule. Subsonically, the boattail of the small-plug nozzle consistently had the highest drag coefficients.

Pressure Ratio Effects

The effect of nozzle pressure ratio on performance characteristics is shown in figures 13 to 15 for all nozzles tested. Efficiencies for the convergent nozzle with $A_8/A_m = 0.10$ were calculated by subtracting the measured boattail and base pressure drag from the ideal internal thrust of a convergent nozzle. For all the boattailed nozzles tested, the ratio of boattail and base drag to ideal thrust $(D_\beta + D_b)/F_{ip}$ tended toward zero as nozzle pressure ratio was increased. This was due to a twofold effect. As the pressure ratio was increased, the ideal gross thrust also increased, thus reducing the ratio $(D_\beta + D_b)/F_{ip}$. In addition, as pressure ratio was increased the boattail drag decreased because of pressurization by the underexpanded jet.

The effect of nozzle pressure ratio on boattail pressure drag coefficient is shown in figure 16. The boattail drag coefficient generally decreased rapidly with increasing nozzle pressure ratio as the nozzles became more underexpanded and the effect of jet pluming increased. An exception to this occurred for the convergent nozzles at Mach 1.97 where the effect of nozzle pressure ratio on boattail drag coefficient was relatively small when compared with the effect at other Mach numbers.

Boattail Pressure Distributions

Figure 17 presents boattail pressure coefficient distributions for all boattailed nozzles tested. As previously stated and as can be seen from this figure, the low boattail drags for these nozzles at subsonic speeds resulted from the relatively high recompression at the trailing edge of these boattails. For the convergent nozzles at a free-stream Mach number of 1.97 the pressure profiles are quite flat for almost the entire length of the boattail.

Plug Pressure Distributions

Figure 18 presents plug pressure distributions for the two plug nozzles tested. Quiescent data are compared to data with external flow at nozzle pressure ratios approximating the assumed nozzle pressure ratio schedule. External flow effects on plug pressure distributions at subsonic Mach numbers were relatively small for the small-plug nozzle. However, for the large-plug nozzle at subsonic speeds these effects became appreciable.

SUMMARY OF RESULTS

A parametric variation of projected boattail area and plug area was conducted to determine the effect on performance characteristics. Three basic nozzles were tested: a convergent nozzle with a circular arc boattail, a plug nozzle with a large conical plug and no boattail, and a plug nozzle with a small conical plug and a circular arc boattail. The small-plug nozzle was designed such that the projected boattail and plug areas were equal. Each of these nozzles had a throat area that was 25 percent of the nacelle area. Two additional convergent nozzles were tested to evaluate effects of throat area variations. Testing was conducted over a range of Mach numbers from 0 to 1.97. The following results were obtained:

1. At a subsonic cruise Mach number of 0.90 and a nozzle pressure ratio of 2.8, the convergent nozzle with a jet-area-to-nacelle area ratio of 0.25 provided better efficiency than either of the two plug nozzles. The convergent nozzle had an efficiency of 98.2 percent compared with 97.3 percent for the small-plug nozzle and 93.9 percent for the large-plug nozzle.

2. The high performance of the convergent nozzle was a result of the low boattail pressure drag. At subsonic speeds the recompression at the trailing edge of the long circular arc boattail resulted in essentially zero boattail drag up to Mach 0.95. The plug force of the small-plug nozzle was near zero at subsonic speeds, but the boattail had a small drag which resulted in slightly lower performance when compared with the convergent nozzle. The low performance of the large-plug nozzle can be directly attributed to the large drag on the plug surface.

3. At a supersonic dash Mach number of 1.97 and a nozzle pressure ratio of 10.7, the convergent nozzle with a jet-area-to-nacelle area ratio of 0.35 had an efficienty of

90.5 percent. At this flight condition, the boattail drag accounted for a 2 percent loss in nozzle efficiency.

Lewis Research Center,
National Aeronautics and Space Administration,
Cleveland, Ohio, June 15, 1970,
720-03.

APPENDIX - SYMBOLS

A	cross-sectional area
C_D	pressure drag coefficient, D/q_0A_m
C_p	pressure coefficient, $(p - p_0)/q_0$
D	drag
d	diameter
F	nozzle gross thrust
F_{pl}	plug force (upstream is positive) measured downstream of throat
$\frac{F - D}{F_{ip}}$	nozzle efficiency
l	length
M	Mach number
P	total pressure
p	static pressure
q	dynamic pressure
r	radius of curvature
x	axial distance downstream of boattail attachment point
x_{pl}	axial distance downstream of nozzle throat
Y	inside diameter of annular base at station 8
y	distance measured along primary flow rake (station 7) from primary airflow passage wall
Z	outside diameter of annular base at station 8
β	boattail trailing-edge angle
θ	internal lip angle at nozzle throat
φ	circumferential angle measured from top of nacelle in a clockwise direction (looking upstream)

Subscripts:

b	base
c	convergent
i	ideal
m	nacelle
p	primary air
pl	plug
β	boattail surface
0	free stream
7	nozzle inlet station
8	nozzle throat station
9	nozzle exit station

REFERENCES

1. Smith, K. G.: Methods and Charts for Estimating Skin Friction Drag in Wind Tunnel Tests With Zero Heat Transfer. Rep. ARC-CP-824, Aeronautical Research Council, Great Britain, 1965.

2. Harrington, Douglas E.: Jet Effects on Boattail Pressure Drag of Isolated Ejector Nozzles at Mach Numbers From 0.60 to 1.47. NASA TM X-1785, 1969.

3. Blaha, Bernard J.; and Bresnahan, Donald L.: Wind Tunnel Installation Effects on Isolated Afterbodies at Mach Numbers From 0.56 to 1.5. NASA TM X-52581, 1969.

4. Schmeer, James W.; Kirkham, Frank S.; and Salters, Leland B., Jr.: Performance Characteristics of a 10^{o} Conical Plug Nozzle at Mach Numbers Up to 1.29. NASA TM X-913, 1964.

5. Bresnahan, Donald L.; and Johns, Albert L.: Cold Flow Investigation of a Low Angle Turbojet Plug Nozzle With Fixed Throat and Translating Shroud at Mach Numbers From 0 to 2.0. NASA TM X-1619, 1968.

6. Wasko, Robert A.; and Harrington, Douglas E.: Performance of a Collapsible Plug Nozzle Having Either Two-Position Cylindrical or Variable Angle Floating Shrouds at Mach Numbers From 0 to 2.0. NASA TM X-1657, 1968.

TABLE I. - NOZZLE VARIABLES

Nozzle configuration[a] and ratio of throat area to nacelle area A_8/A_m	Boattail projected area to nacelle area, A_β/A_m	Base area to nacelle area, A_b/A_m	Plug projected area to nacelle area, A_{pl}/A_m	Boattail trailing-edge angle, β, deg	Boattail length to nacelle diameter, l_β/d_m	Boattail radius of curvature to nacelle diameter, r_β/d_m
Convergent, 0.10	0.892	0.008	-----	17.3	2.23	7.5
Convergent, 0.25	.738	.012	-----	14.5	1.91	7.5
Convergent, 0.35	.636	.014	-----	13.3	1.71	7.5
Small plug, 0.25	.356	.019	0.375	9.0	1.27	8.0
Large plug, 0.25	0	.028	.722	----	----	---

[a]See fig. 4.

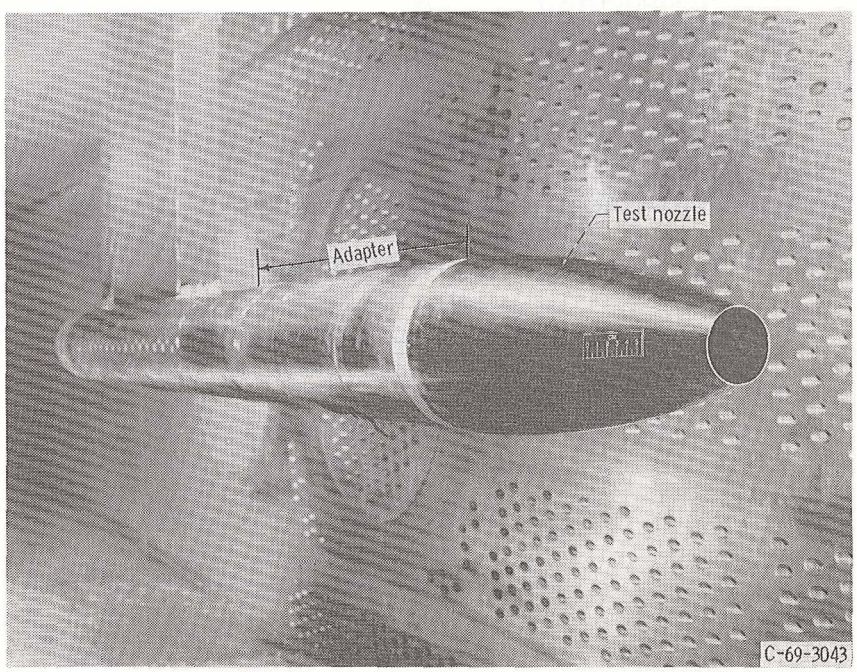

Figure 1. - Model installed in 8- by 6-Foot Supersonic Wind Tunnel.

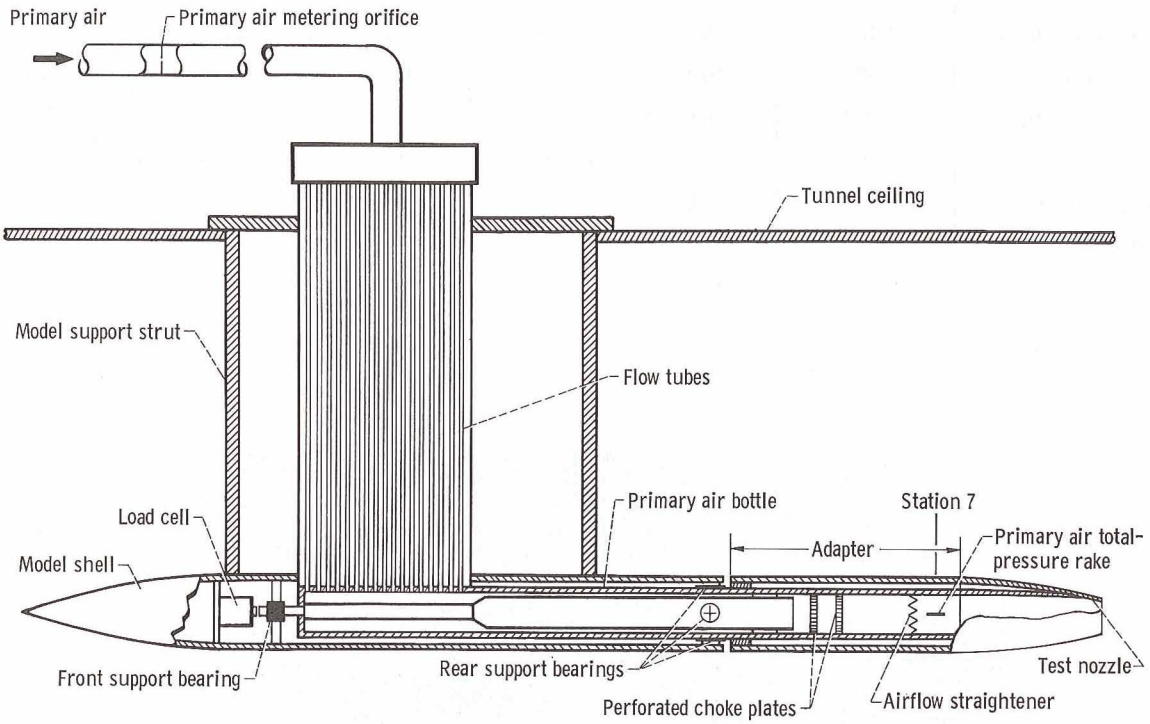

Figure 2. - Model internal geometry and thrust-measuring system. CD-10813-28

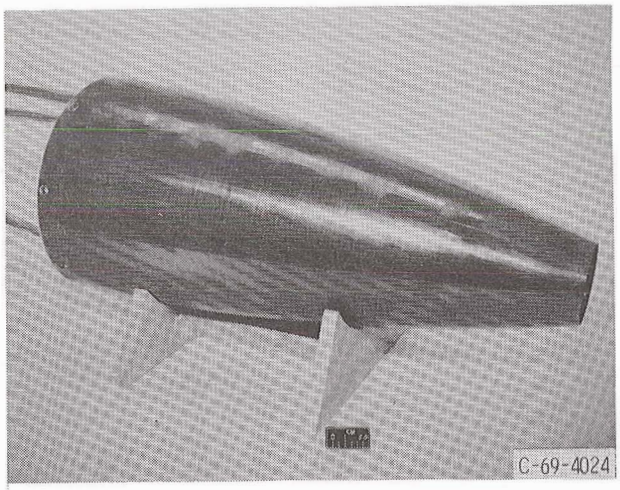

(a) Convergent; $A_8/A_m = 0.10$.

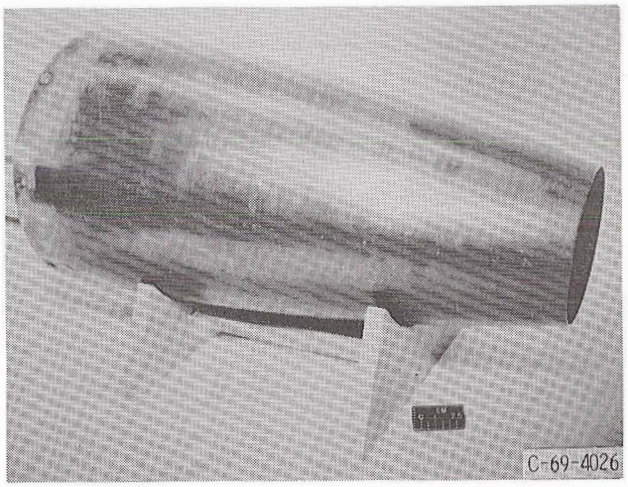

(b) Convergent; $A_8/A_m = 0.25$.

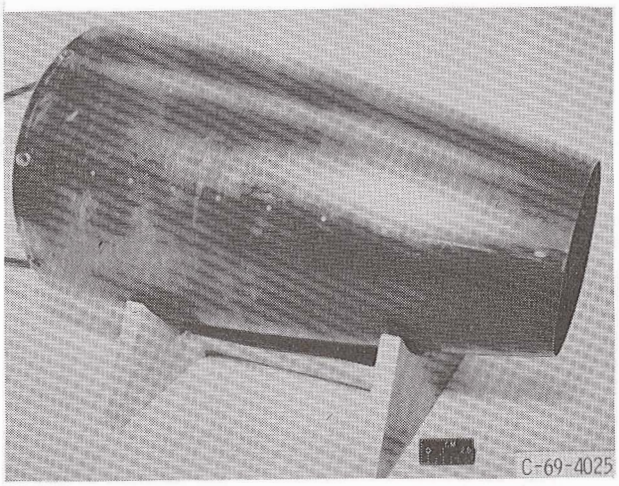

(c) Convergent; $A_8/A_m = 0.35$.

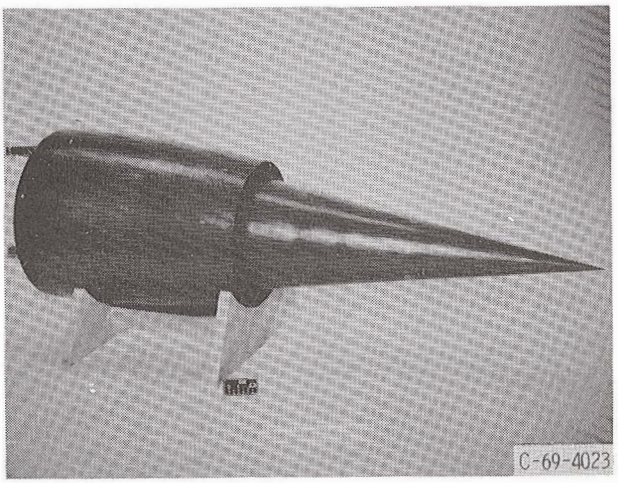

(d) Small plug; $A_8/A_m = 0.25$.

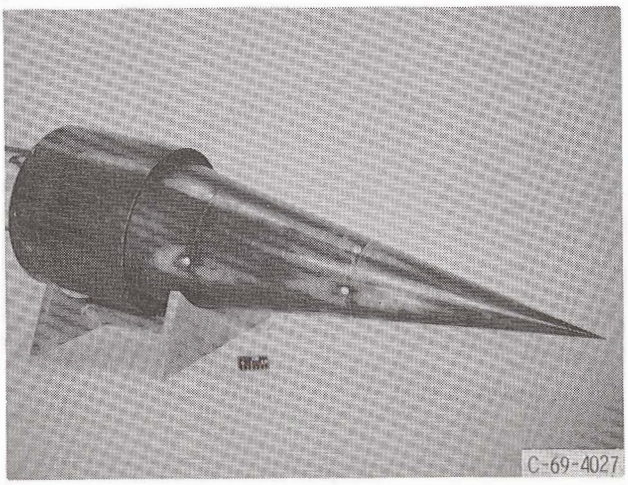

(e) Large plug; $A_8/A_m = 0.25$.

Figure 3. - Test nozzles. Various configurations and ratios of nozzle throat area to nacelle area A_8/A_m.

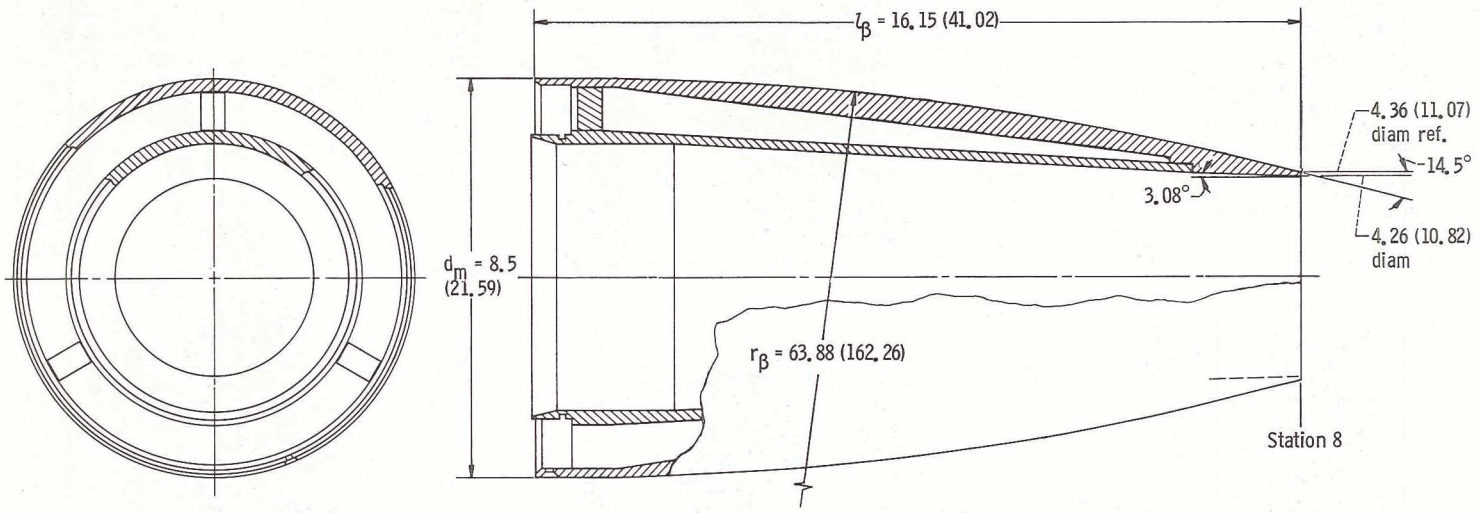

(a) Convergent nozzle; A_8/A_m = 0.25.

CD-10808-28

Figure 4. - Model dimensions and geometric variables (see table I). (All dimensions are in inches (cm)).

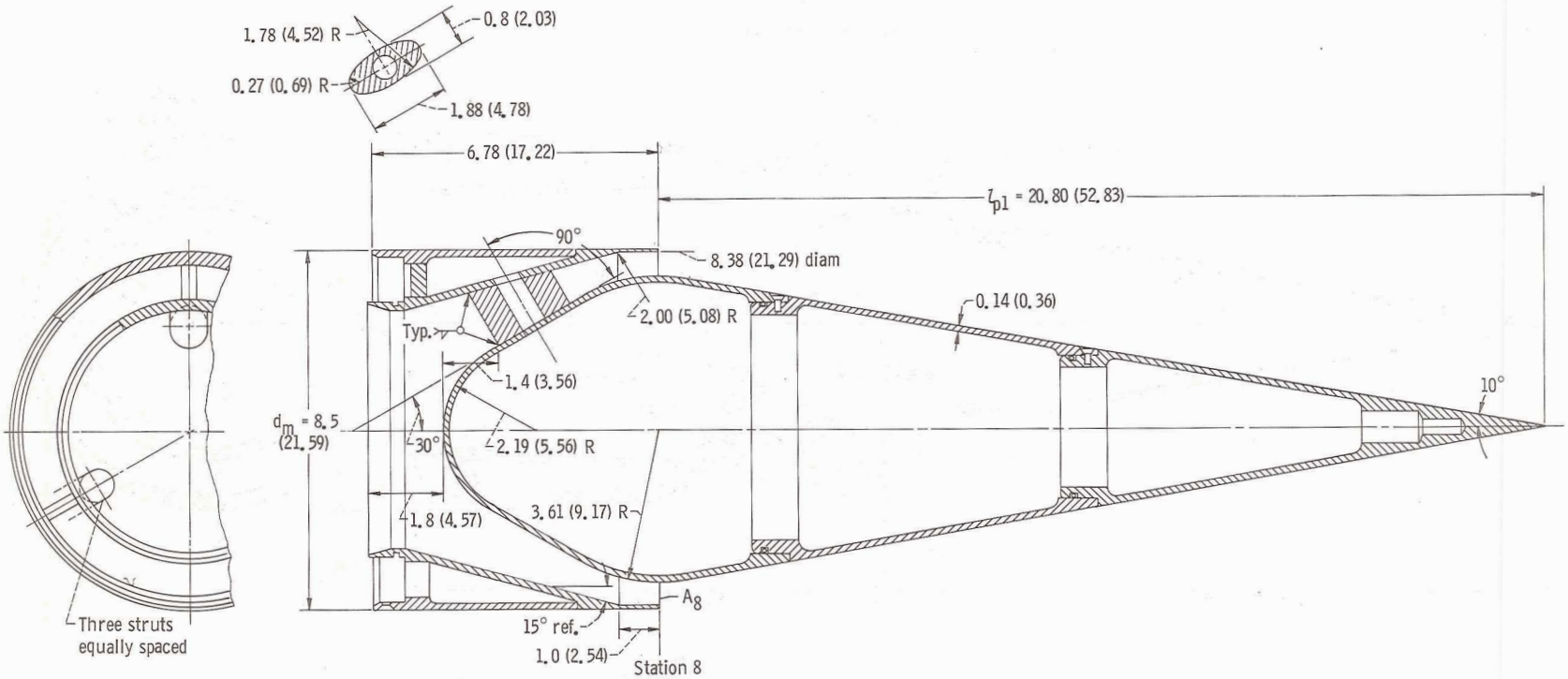

(b) Large-plug nozzle; A_8/A_m = 0.25.

CD-10811-28

Figure 4. - Continued.

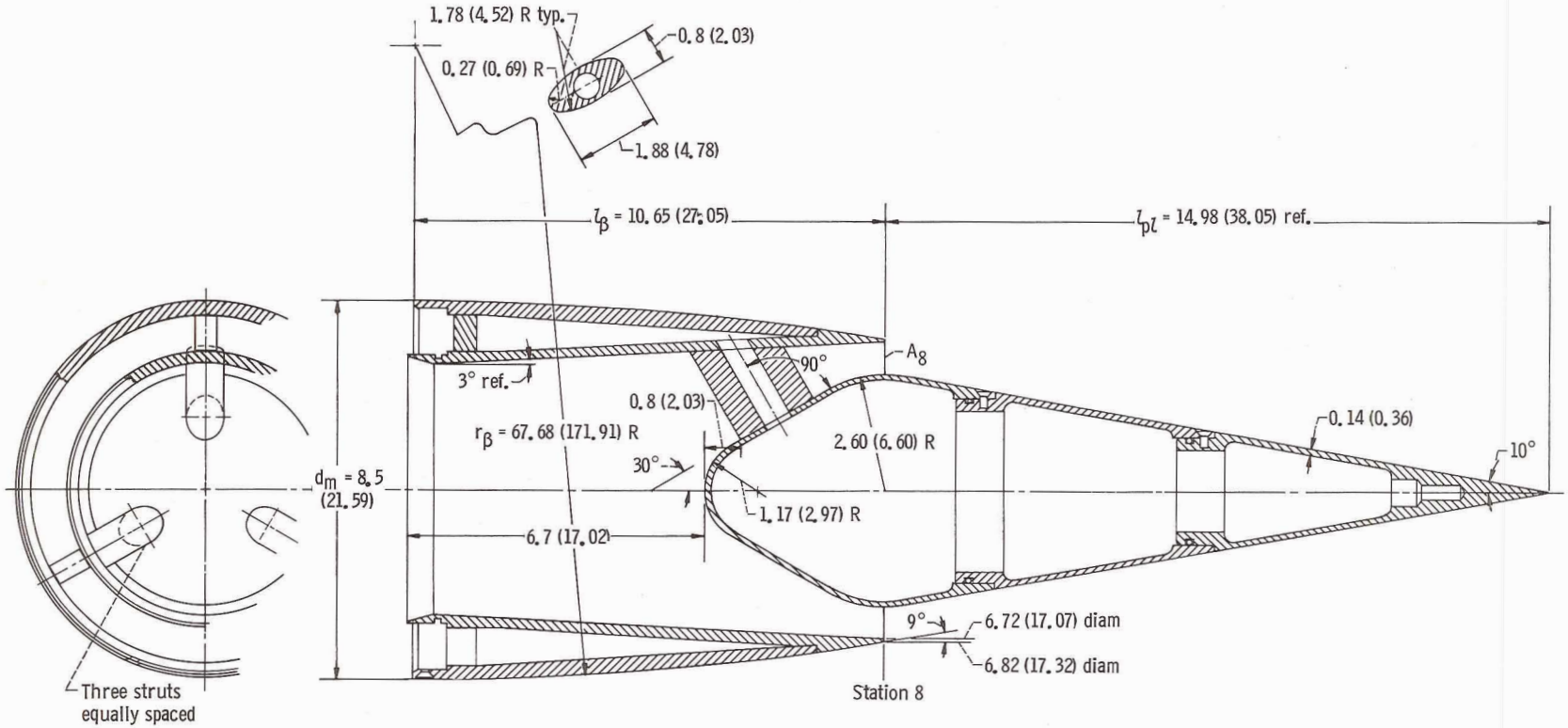

(c) Small-plug nozzle; A_8/A_m = 0.25.

CD-10812-28

Figure 4. - Continued.

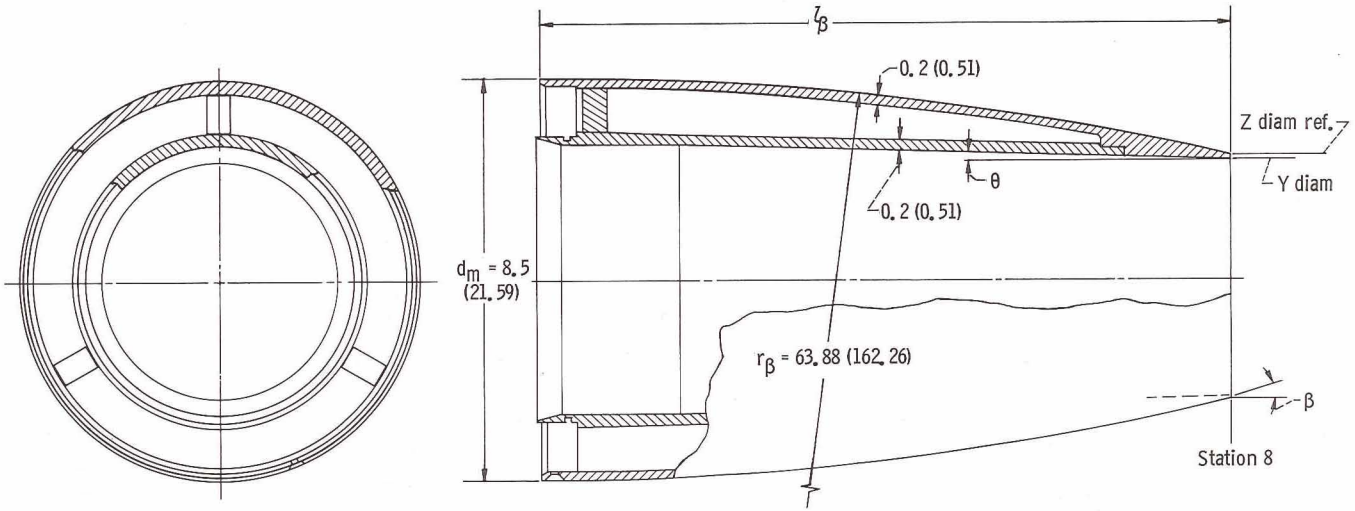

Nozzle configuration and ratio of nozzle throat area to nacelle area A_8/A_m	Internal flow angle, θ, deg	Boattail angle, β, deg	Boattail length, l_β		Inside base diameter, Y		Outside base diameter, Z	
			in.	cm	in.	cm	in.	cm
Convergent, 0.10	1.62	17.3	14.65	37.21	5.03	12.78	5.13	13.03
Convergent, 0.35	5.37	13.3	18.97	48.18	2.69	6.83	2.79	7.09

(d) Convergent nozzle; A_8/A_m = 0.10 and A_8/A_m = 0.35.

CD-10810-28

Figure 4. - Concluded.

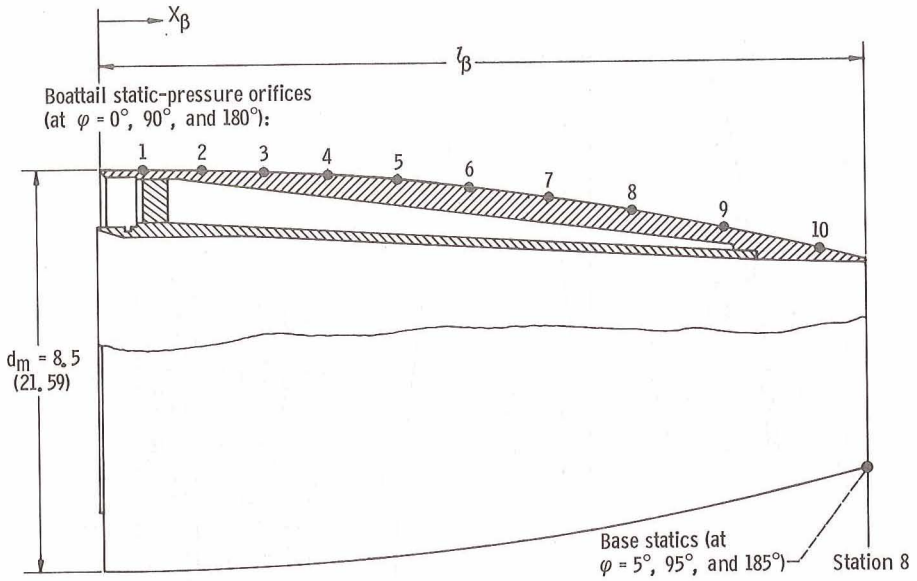

Boattail static-pressure locations			
Orifice number	Ratio of nozzle throat area to nacelle area, A_8/A_m		
	0.10	0.25	0.35
	Ratio of boattail length to nacelle diameter, l_β/d_m		
	2.22	1.90	1.71
	Ratio of boattail axial distance to model diameter, X_β/d_m		
1	0.17	0.12	0.16
2	.32	.27	.30
3	.47	.42	.44
4	.64	.58	.58
5	.81	.74	.73
6	1.00	.92	.89
7	1.21	1.11	1.05
8	1.44	1.31	1.22
9	1.71	1.53	1.41
10	2.02	1.77	1.61

CD-10806-28

(a) Convergent nozzles.

Figure 5. - Nozzle static-pressure instrumentation. (All dimensions are in inches (cm)).

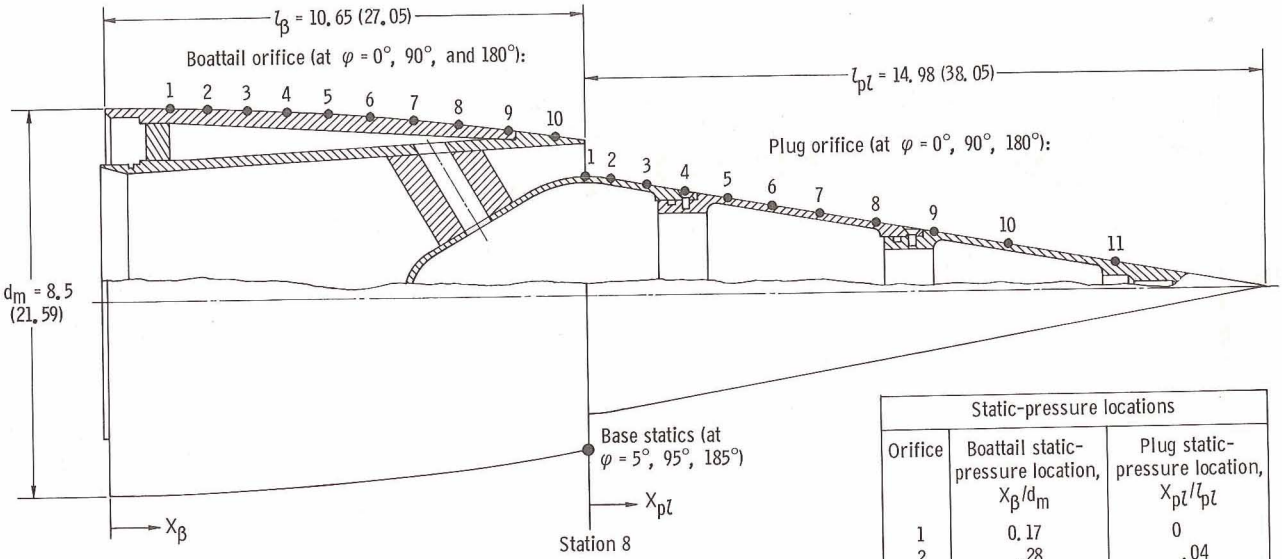

Static-pressure locations		
Orifice	Boattail static-pressure location, X_β/d_m	Plug static-pressure location, X_{pl}/l_{pl}
1	0.17	0
2	.28	.04
3	.38	.09
4	.49	.15
5	.60	.21
6	.71	.27
7	.83	.34
8	.95	.42
9	1.07	.51
10	1.19	.62
11	----	.78

(b) Small-plug nozzle; A_8/A_m = 0.25.

CD-10807-28

Figure 5. - Continued.

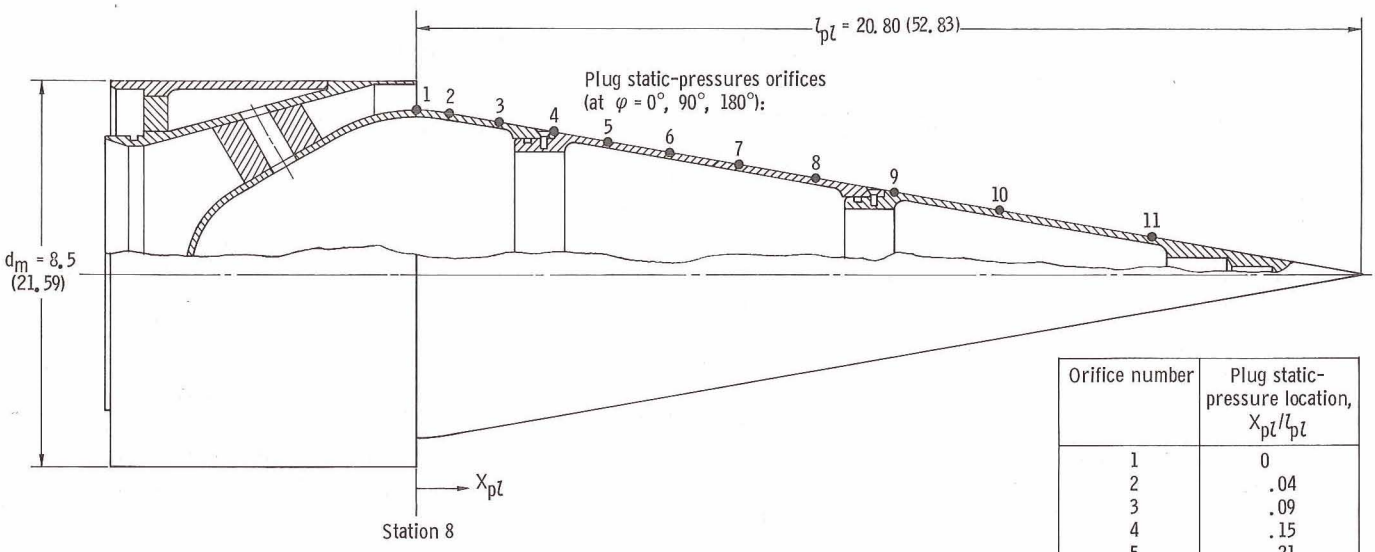

Orifice number	Plug static-pressure location, X_{pl}/l_{pl}
1	0
2	.04
3	.09
4	.15
5	.21
6	.27
7	.34
8	.42
9	.51
10	.62
11	.78

(c) Large-plug nozzle; A_8/A_m = 0.25.

CD-10809-28

Figure 5. - Concluded.

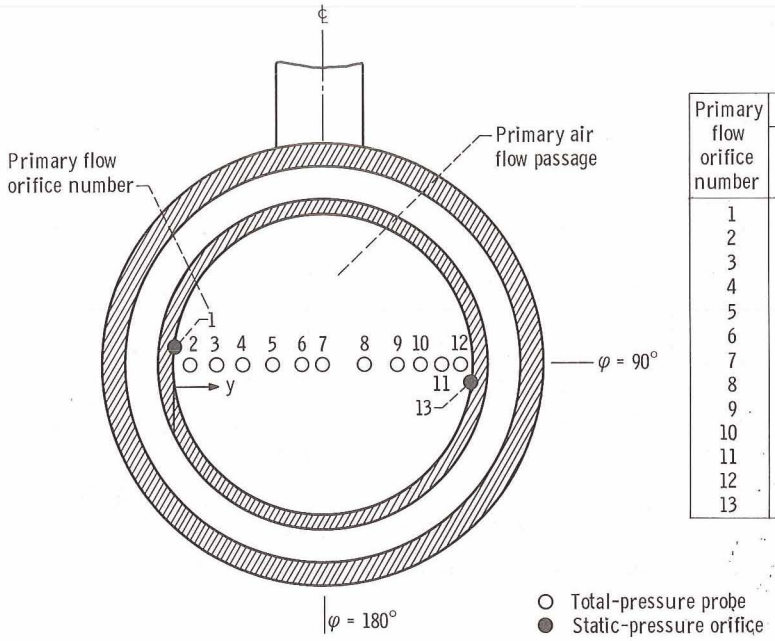

Primary flow orifice number	y	
	in.	cm
1	0	0
2	.29	.74
3	.61	1.55
4	.98	2.49
5	1.43	3.63
6	2.10	5.34
7	3.00	7.61
8	4.28	10.88
9	4.81	12.21
10	5.23	13.28
11	5.56	14.12
12	5.87	14.90
13	6.01	15.27

Figure 6. - Primary air total-pressure instrumentation. (All dimensions are in inches (cm).)

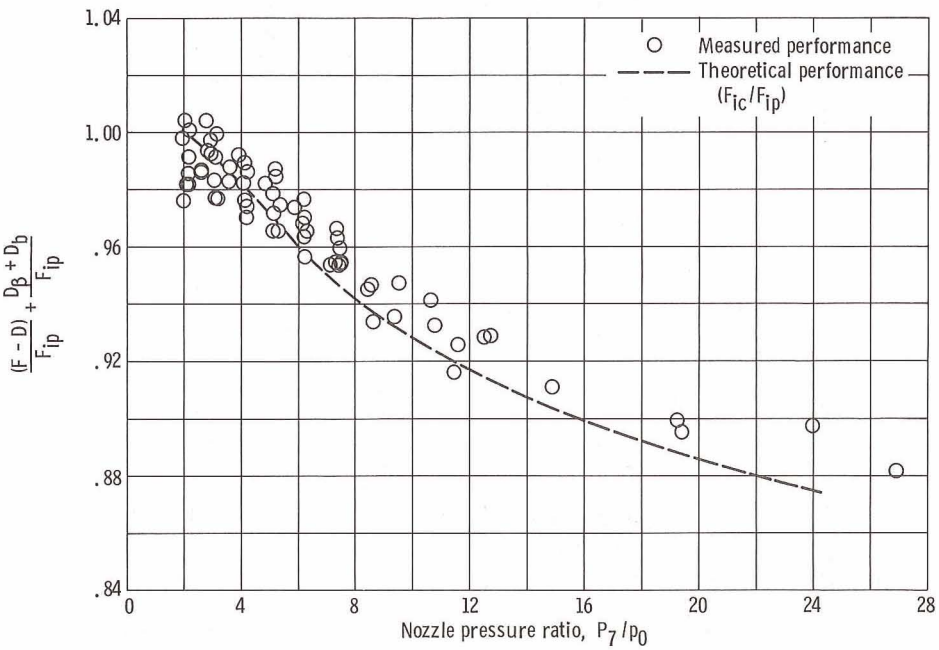

Figure 7. - Comparison of measured and theoretical internal performance of convergent nozzles with nozzle-throat-area-to-nacelle-area ratios of 0.25 and 0.35.

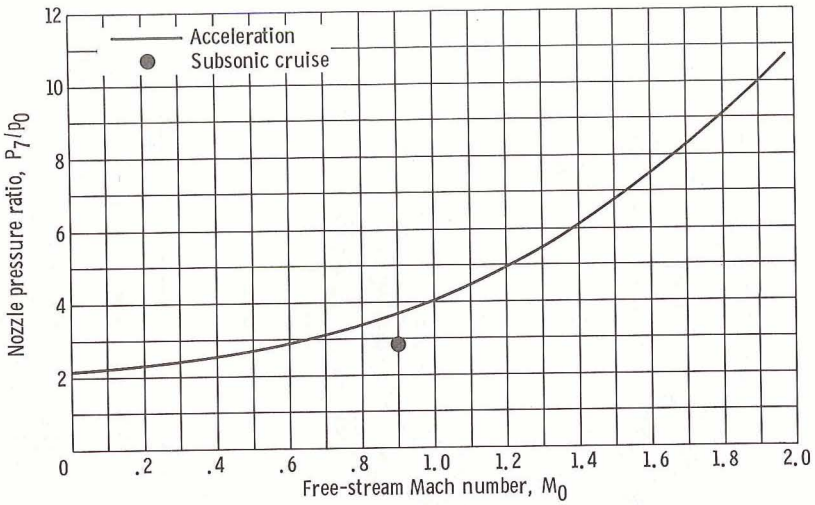

Figure 8. - Assumed turbofan pressure ratio schedule.

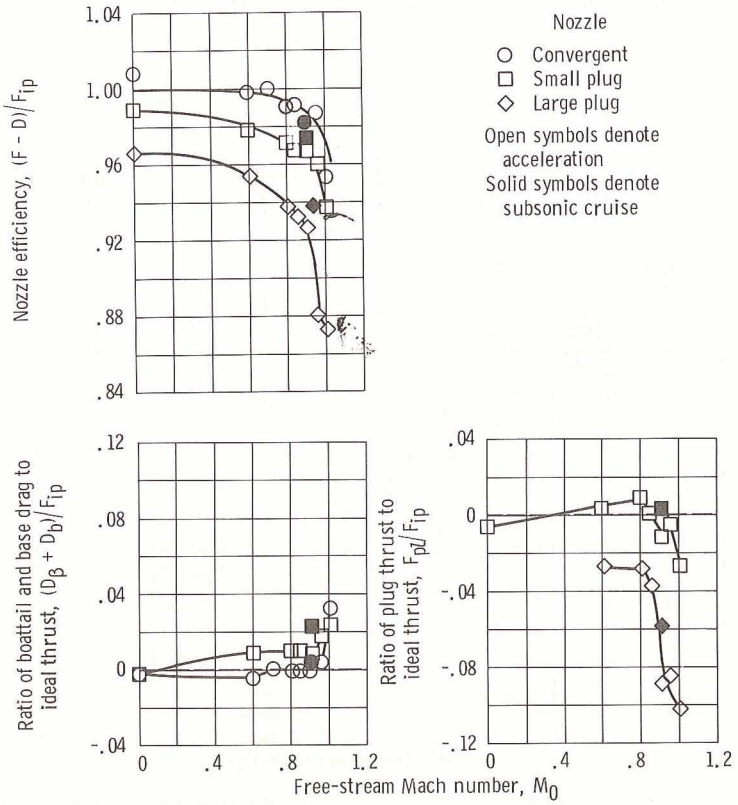

Figure 9. - Comparison of plug and boattail convergent nozzles (using assumed turbofan pressure ratio schedule). Ratio of nozzle throat area to nacelle area, 0.25.

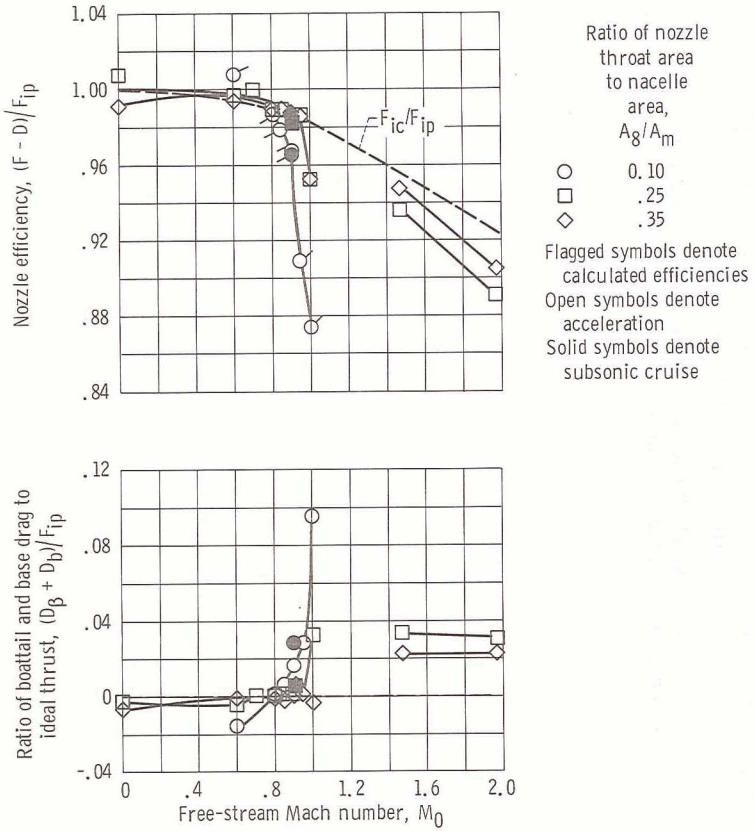

Figure 10. - Effect of throat area variation on performance characteristics of convergent nozzles (using assumed turbofan pressure ratio schedule).

Reference	Internal lip angle, θ, deg	Internal expansion area ratio, A_9/A_8	Ratio of nozzle throat area to nacelle area, A_8/A_m	Ratio of projected plug area to nacelle area, A_{pl}/A_m
○ Present study, large plug	0	1.00	0.25	0.722
▱ Present study, small plug	0	1.00	.25	.375
△ Ref. 4	6	1.00	.24	.43
□ Ref. 5	0	1.12	.26	.625
◇ Ref. 6	8	1.00	.26	.59

Open symbols denote acceleration
Solid symbols denote subsonic cruise

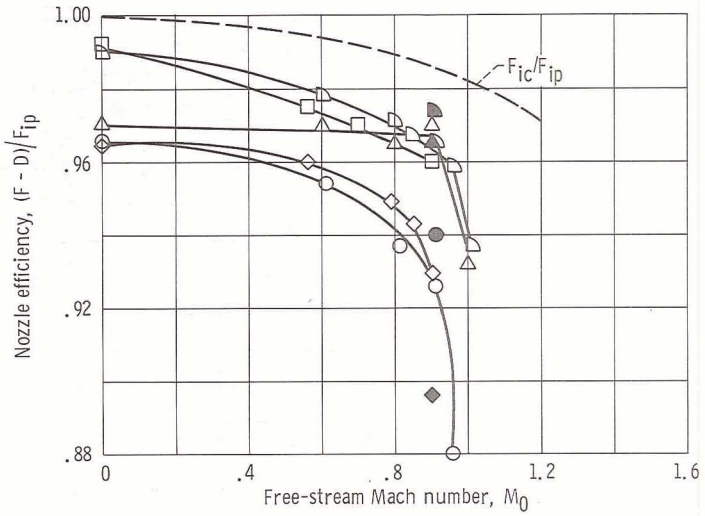

Figure 11. - Comparison of plug nozzle efficiencies.

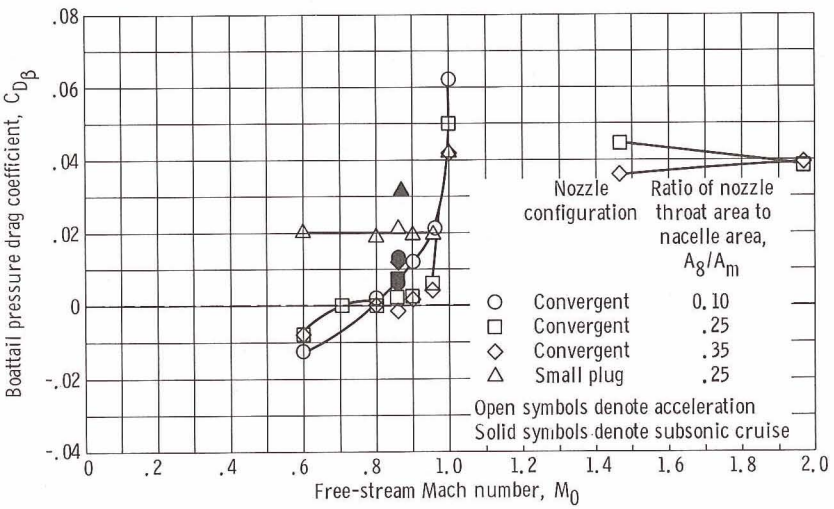

Figure 12. - Comparison of boattail pressure drag coefficients for boattail nozzles (using assumed turbofan pressure ratio schedule).

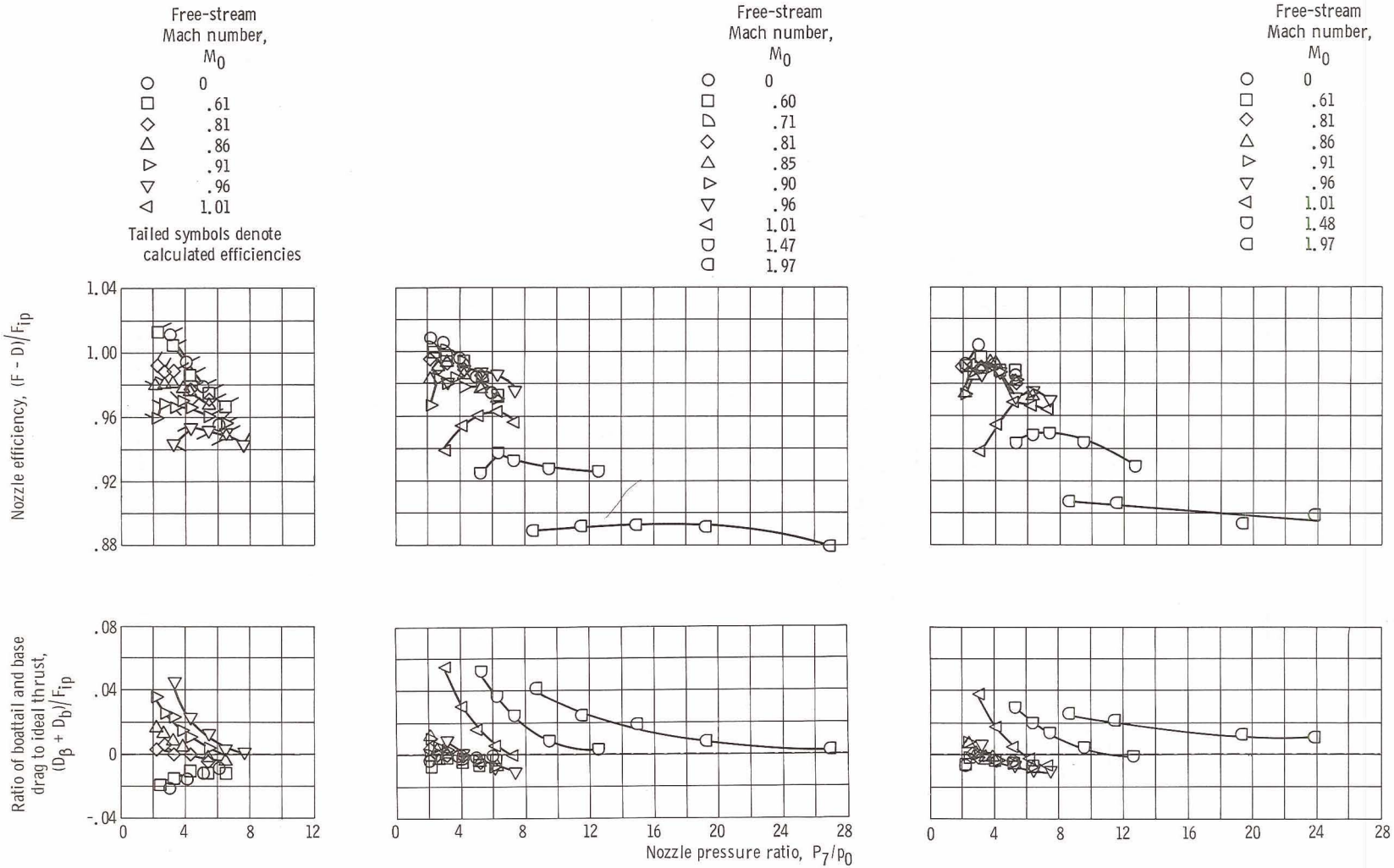

(a) Ratio of nozzle throat area to nacelle area, 0.10.

(b) Ratio of nozzle throat area to nacelle area, 0.25.

(c) Ratio of nozzle throat area to nacelle area, 0.35.

Figure 13. - Effect of nozzle pressure ratio on performance characteristics of convergent nozzles.

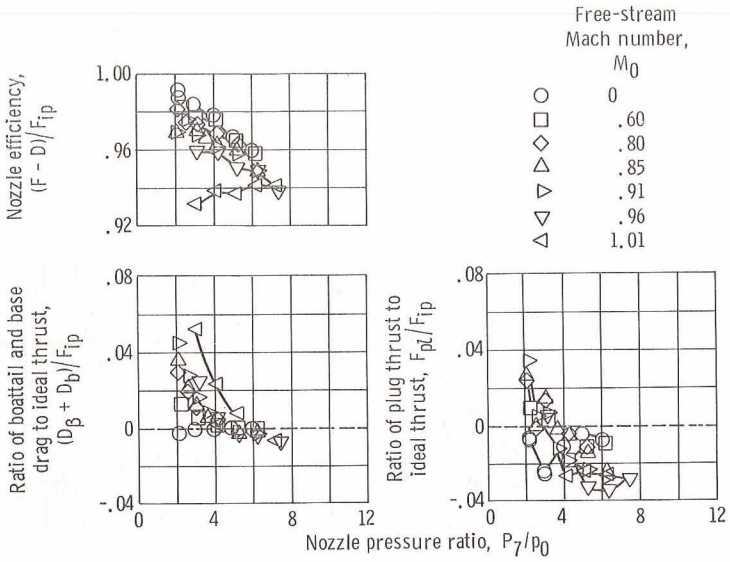

Figure 14. - Effect of nozzle pressure ratio on performance characteristics of small-plug nozzle. Ratio of nozzle throat area to nacelle area, 0.25.

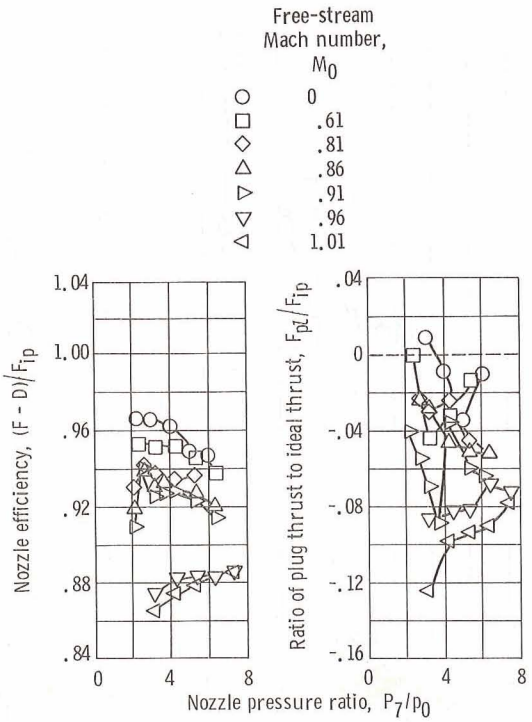

Figure 15. - Effect of nozzle pressure ratio on performance characteristics of large-plug nozzle. Ratio of nozzle throat area to nacelle area, 0.25.

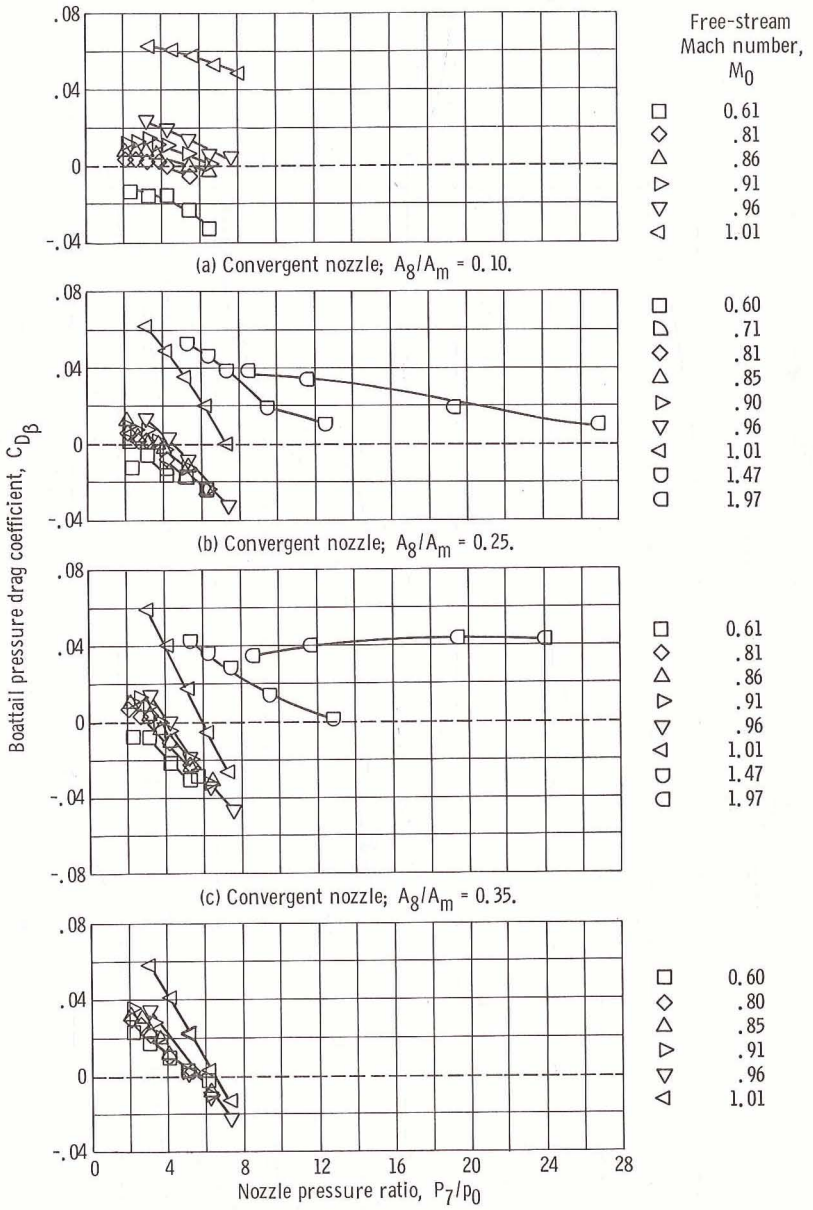

Figure 16. - Effect of nozzle pressure ratio on boattail pressure drag coefficient for various nozzle configurations and ratios of nozzle throat area to nacelle area A_8/A_m.

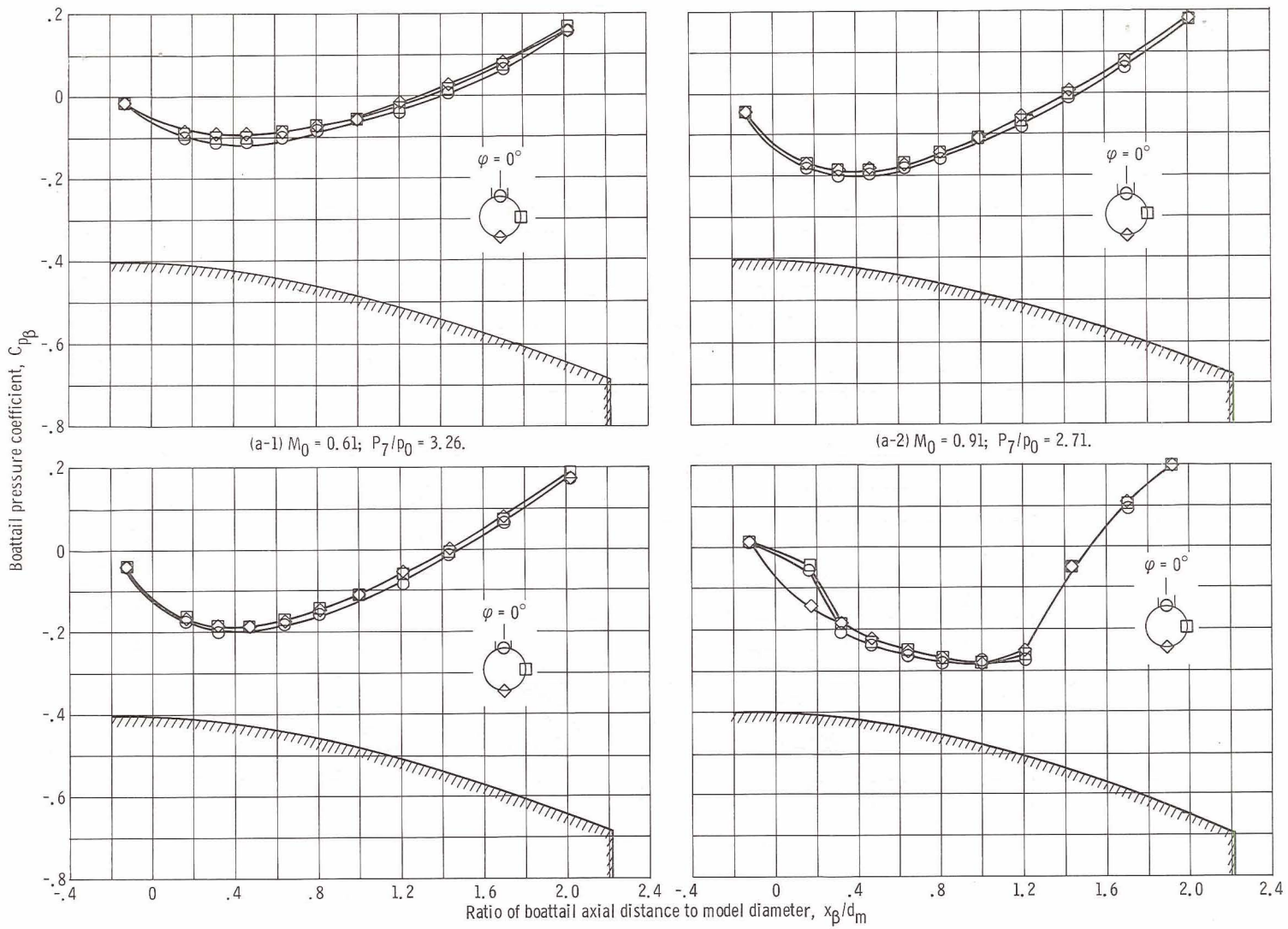

(a-1) $M_0 = 0.61$; $P_7/p_0 = 3.26$.

(a-2) $M_0 = 0.91$; $P_7/p_0 = 2.71$.

(a-3) $M_0 = 0.91$; $P_7/p_0 = 3.80$.

(a-4) $M_0 = 1.01$; $P_7/p_0 = 3.76$.

(a) Convergent nozzle; $A_8/A_m = 0.10$.

Figure 17. - Boattail pressure coefficient distributions for various nozzle configurations, ratios of nozzle throat area to nacelle area A_8/A_m, free-stream Mach numbers M_0, and nozzle pressure ratios P_7/p_0.

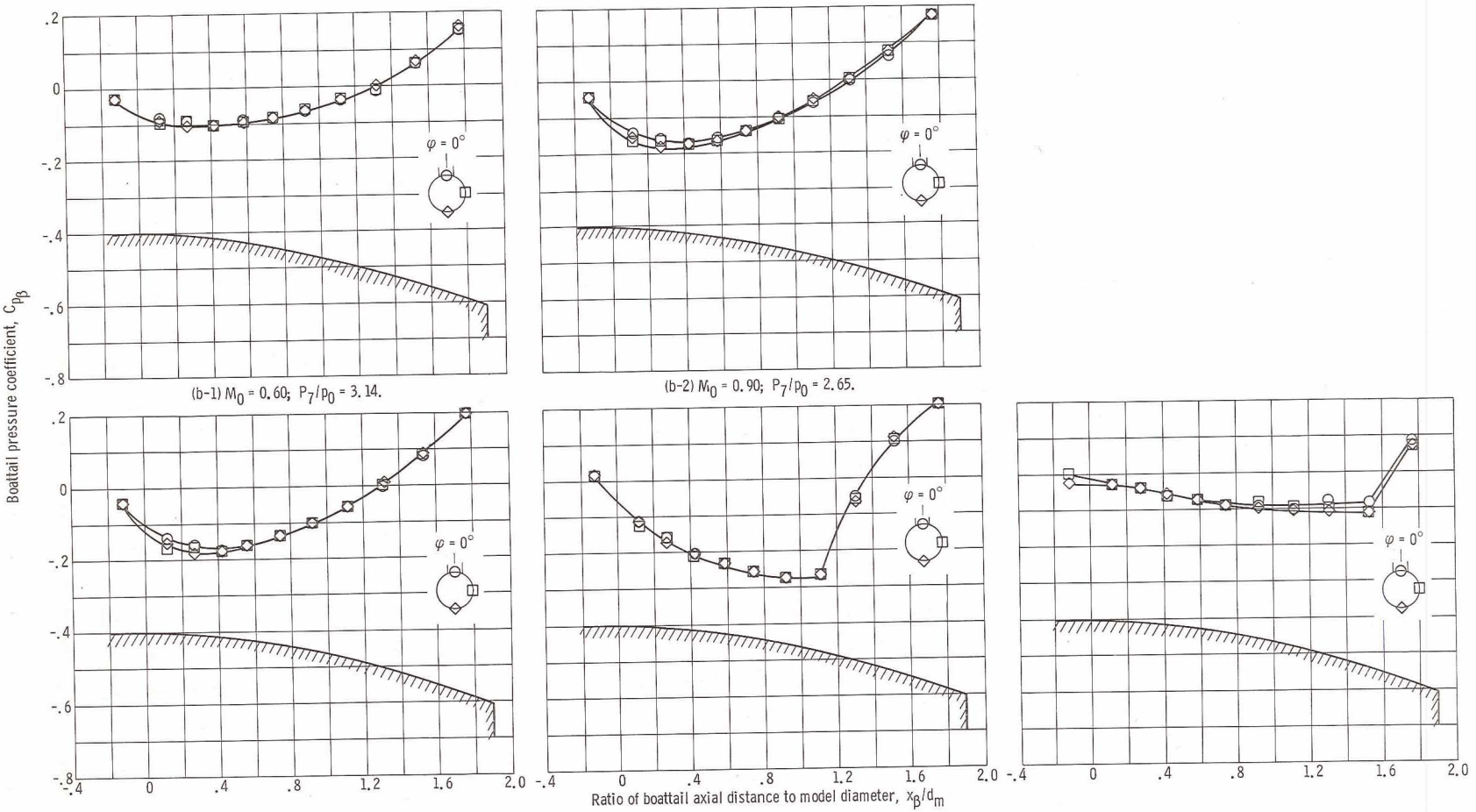

(b-1) $M_0 = 0.60$; $P_7/p_0 = 3.14$.

(b-2) $M_0 = 0.90$; $P_7/p_0 = 2.65$.

(b-3) $M_0 = 0.90$; $P_7/p_0 = 3.69$.

(b-4) $M_0 = 1.01$; $P_7/p_0 = 3.14$.

(b-5) $M_0 = 1.97$; $P_7/p_0 = 11.56$.

(b) Convergent nozzle; $A_8/A_m = 0.25$.

Figure 17. - Continued.

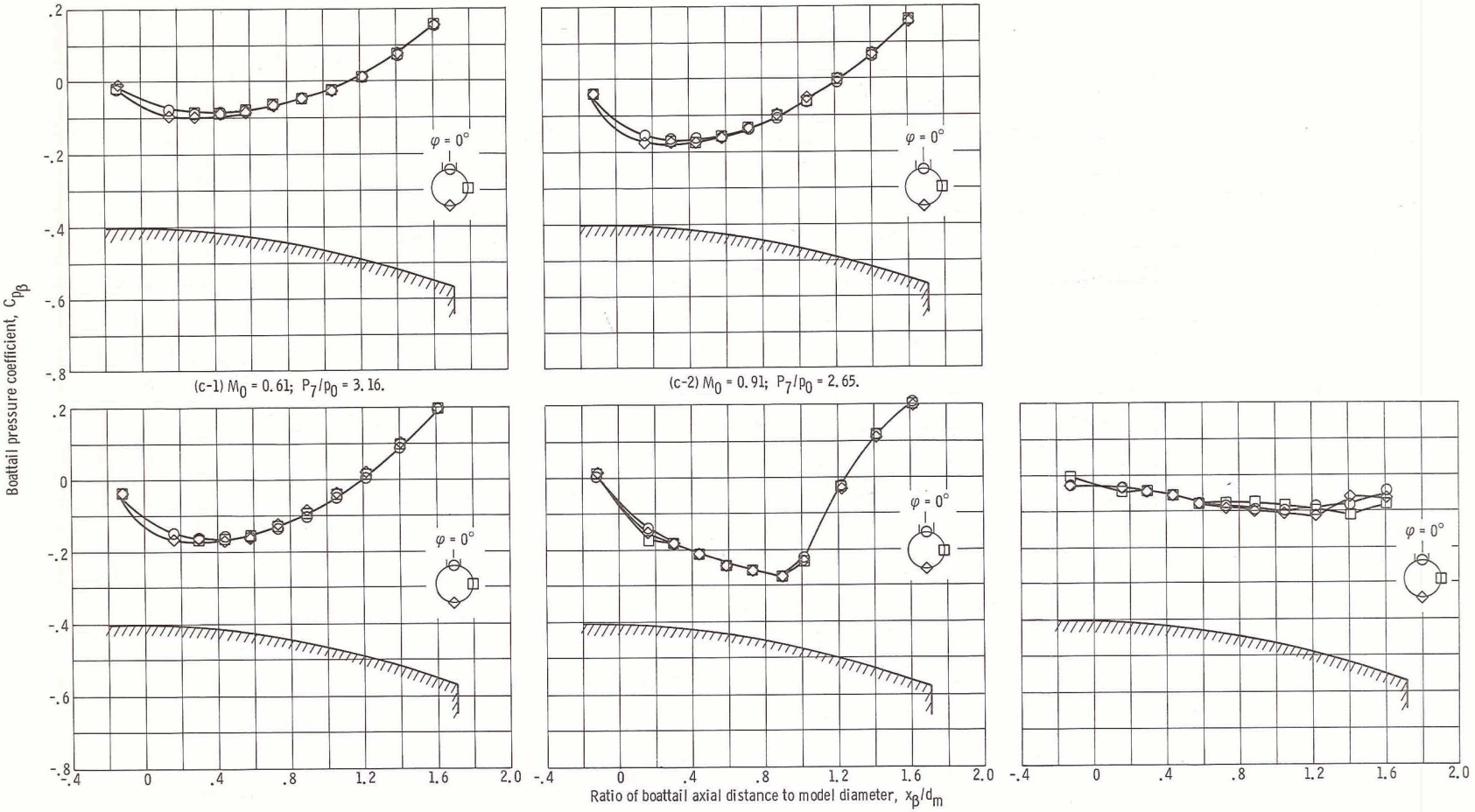

(c-1) $M_0 = 0.61$; $P_7/p_0 = 3.16$.

(c-2) $M_0 = 0.91$; $P_7/p_0 = 2.65$.

(c-3) $M_0 = 0.91$; $P_7/p_0 = 3.72$.

(c-4) $M_0 = 1.01$; $P_7/p_0 = 4.22$.

(c-5) $M_0 = 1.97$; $P_7/p_0 = 11.55$.

(c) Convergent nozzle; $A_8/A_m = 0.35$.

Figure 17. - Continued.

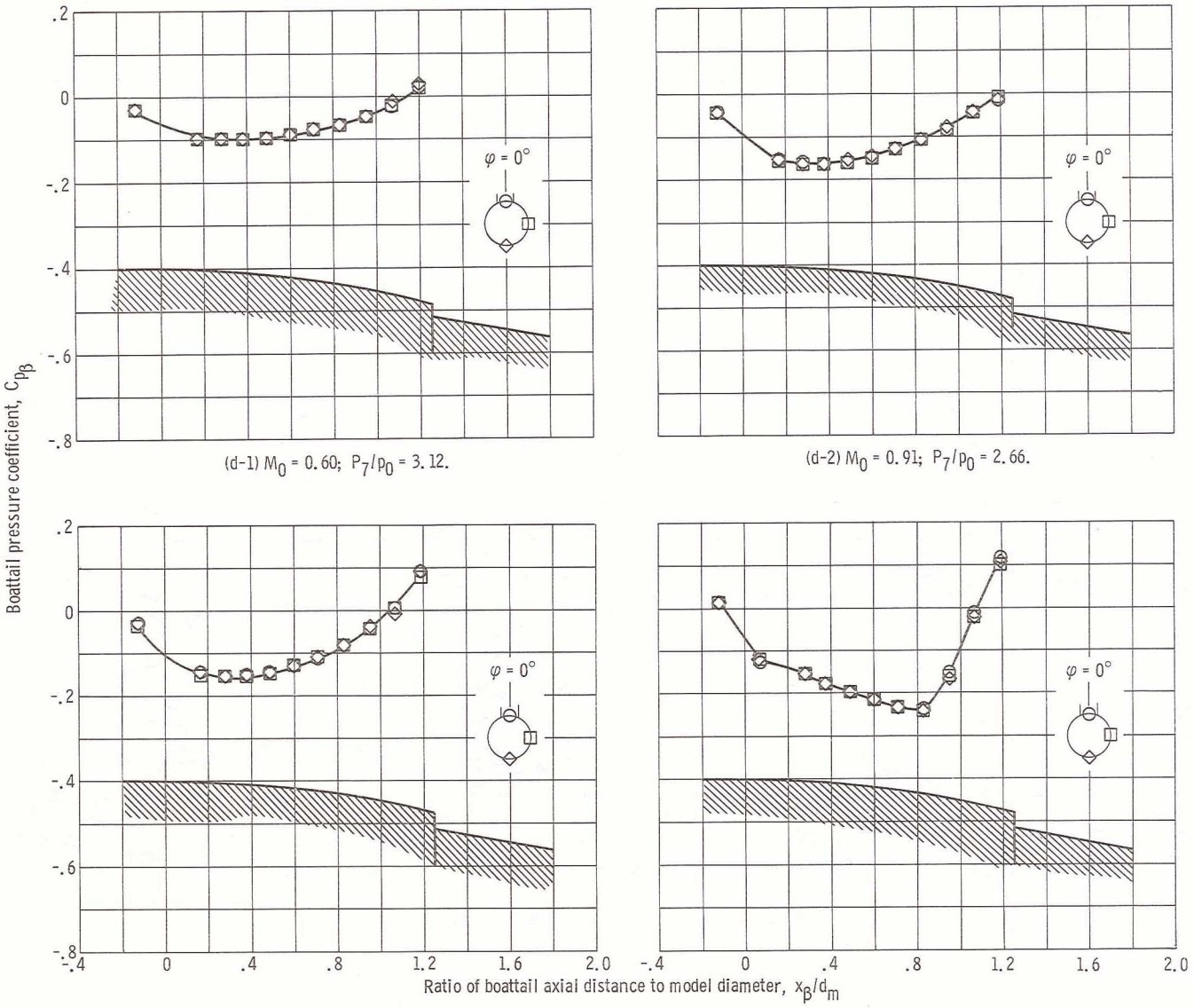

(d-1) $M_0 = 0.60$; $P_7/p_0 = 3.12$.

(d-2) $M_0 = 0.91$; $P_7/p_0 = 2.66$.

(d-3) $M_0 = 0.91$; $P_7/p_0 = 3.71$.

(d-4) $M_0 = 1.01$; $P_7/p_0 = 4.21$.

(d) Small-plug nozzle; $A_8/A_m = 0.25$.

Figure 17. - Concluded.

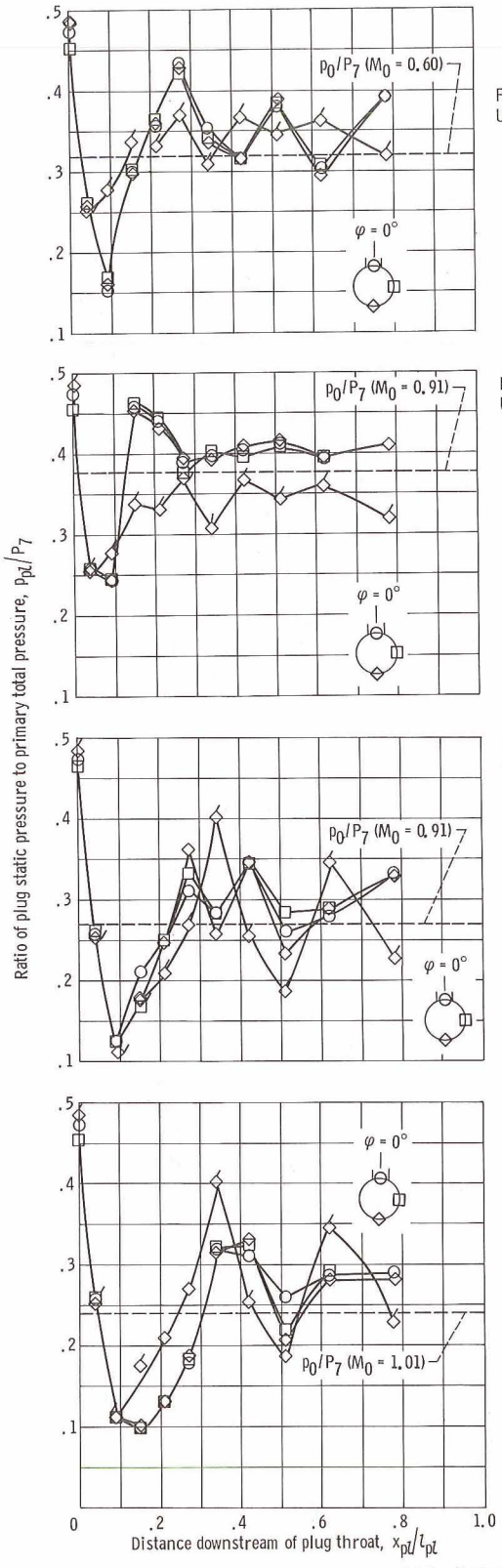

	Free-stream Mach number, M_0	Nozzle pressure ratio, P_7/p_0
Flagged symbols	0	2.98
Unflagged symbols	.60	3.12
Flagged symbols	0	2.98
Unflagged symbols	.91	2.66
Flagged symbols	0	3.98
Unflagged symbols	.91	3.71
Flagged symbols	0	3.98
Unflagged symbols	1.01	4.21

(a) Small-plug nozzle.

Figure 18. - Plug pressure distributions. Ratio of nozzle throat area to nacelle area, A_8/A_m = 0.25.

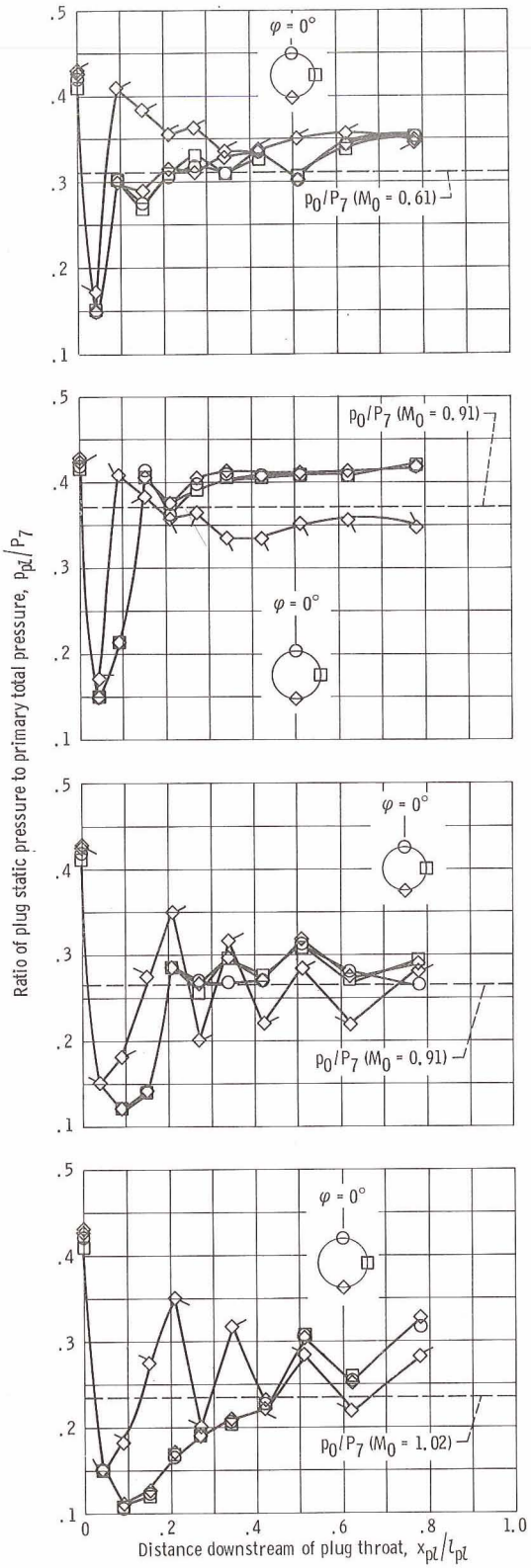

	Free-stream Mach number, M_0	Nozzle pressure ratio, P_7/p_0
Flagged symbols	0	3.00
Unflagged symbols	.61	3.20
Flagged symbols	0	3.00
Unflagged symbols	.91	2.69
Flagged symbols	0	4.01
Unflagged symbols	.91	3.74
Flagged symbols	0	4.01
Unflagged symbols	1.02	4.26

(b) Large-plug nozzle.

Figure 18. - Concluded.

NATIONAL AERONAUTICS AND SPACE ADMINISTRATION
WASHINGTON, D. C. 20546

OFFICIAL BUSINESS

FIRST CLASS MAIL

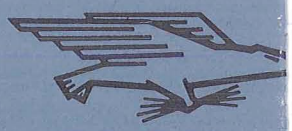

"The aeronautical and space activities of the United States shall be conducted so as to contribute . . . to the expansion of human knowledge of phenomena in the atmosphere and space. The Administration shall provide for the widest practicable and appropriate dissemination of information concerning its activities and the results thereof."

—NATIONAL AERONAUTICS AND SPACE ACT OF 1958

NASA SCIENTIFIC AND TECHNICAL PUBLICATIONS

TECHNICAL REPORTS: Scientific and technical information considered important, complete, and a lasting contribution to existing knowledge.

TECHNICAL NOTES: Information less broad in scope but nevertheless of importance as a contribution to existing knowledge.

TECHNICAL MEMORANDUMS: Information receiving limited distribution because of preliminary data, security classification, or other reasons.

CONTRACTOR REPORTS: Scientific and technical information generated under a NASA contract or grant and considered an important contribution to existing knowledge.

TECHNICAL TRANSLATIONS: Information published in a foreign language considered to merit NASA distribution in English.

SPECIAL PUBLICATIONS: Information derived from or of value to NASA activities. Publications include conference proceedings, monographs, data compilations, handbooks, sourcebooks, and special bibliographies.

TECHNOLOGY UTILIZATION PUBLICATIONS: Information on technology used by NASA that may be of particular interest in commercial and other non-aerospace applications. Publications include Tech Briefs, Technology Utilization Reports and Notes, and Technology Surveys.

Details on the availability of these publications may be obtained from:

SCIENTIFIC AND TECHNICAL INFORMATION DIVISION

NATIONAL AERONAUTICS AND SPACE ADMINISTRATION

Washington, D.C. 20546